

# Dataset Distillation via Relative Distribution Matching and Cognitive Heritage

Qianxin Xia<sup>1</sup> Jiawei Du<sup>\*2</sup> Yuhan Zhang<sup>3</sup> Jielei Wang<sup>1</sup> Guoming Lu<sup>1</sup>

## Abstract

Dataset distillation seeks to synthesize a highly compact dataset that achieves performance comparable to the original dataset on downstream tasks. For the classification task that use pre-trained self-supervised models as backbones, previous linear gradient matching optimizes synthetic images by encouraging them to mimic the gradient updates induced by real images on the linear classifier. However, this batch-level formulation requires loading thousands of real images and applying multiple rounds of differentiable augmentations to synthetic images at each distillation step, leading to substantial computational and memory overhead. In this paper, we introduce statistical flow matching, a stable and efficient supervised learning framework that optimizes synthetic images by aligning constant statistical flows from target class centers to non-target class centers in the original data. Our approach loads raw statistics only once and performs a single augmentation pass on the synthetic data, achieving performance comparable to or better than the state-of-the-art methods with 10x lower GPU memory usage and 4x shorter runtime. Furthermore, we propose a classifier inheritance strategy that reuses the classifier trained on the original dataset for inference, requiring only an extremely lightweight linear projector and marginal storage while achieving substantial performance gains.

## 1. Introduction

In machine learning, data serves as the “fuel” that drives improvements in model capabilities. As datasets grow larger and more diverse, systems can learn richer patterns and achieve better performance. However, this reliance on data

<sup>1</sup>Department of XXX, University of YYY, Location, Country

<sup>2</sup>Company Name, Location, Country

<sup>3</sup>School of ZZZ, Institute of WWW, Location, Country. Correspondence to: Firstname1 Lastname1 <first1.lastname1@xxx.edu>, Firstname2 Lastname2 <first2.lastname2@www.uk>.

Preprint. February 6, 2026.

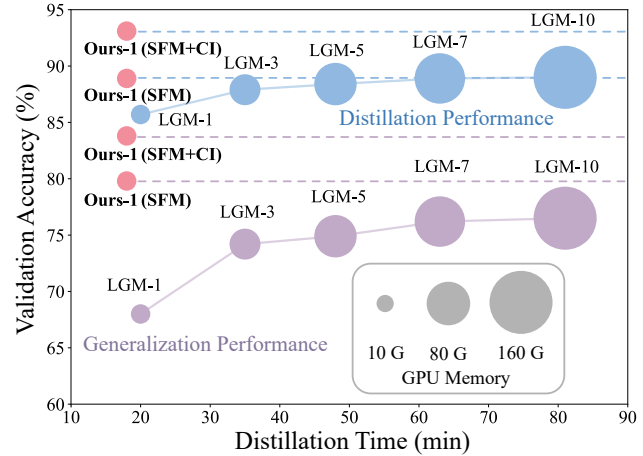


Figure 1. Comparison between LGM and our method (SFM and CI) in terms of distillation time, GPU memory usage, and validation accuracy. The number following each method denotes the augmentations per batch. The distillation model is EVA-02 and the generalized models are CLIP, DINO-v2 and MoCo-v3. Our SFM substantially reduces resource consumption while achieving state-of-the-art validation performance. Furthermore, incorporating CI for evaluation further elevates performance to a higher level.

also introduces significant practical overheads, since large-scale dataset acquisition, management, transmission, and processing require substantial storage, communication and compute capacity (Lei & Tao, 2023). To reconcile high performance with prohibitive resource costs, dataset distillation (DD) (Wang et al., 2018) has been proposed to compresses a cumbersome dataset into a compact surrogate that yields training efficacy comparable to using the full dataset.

Several recent methods (Zhao & Bilen, 2023; Cazenavette et al., 2022; Yin et al., 2023; Su et al., 2024) and their extensions (Wang et al., 2025; Du et al., 2023; Shao et al., 2024; Chan-Santiago et al., 2025) have advanced the ambitious goal of learning high-quality models from synthetic images. However, they typically require distilling a relatively large Image-Per-Class (IPC) and training models from scratch to achieve competitive performance, both of which are inefficient and limits practical training and deployment in specific scenarios, such as resource-constrained edge environments. Consequently, there is an urgent need to investigate a more efficient, practice-ready scheme to break this impasse.

Fortunately, computer vision has increasingly shifted toward

exploiting representations learned by large-scale pre-trained self-supervised vision models (e.g., DINO (Oquab et al., 2023) and CLIP (Radford et al., 2021)) for downstream tasks. In practice, such models are either lightly fine-tuned on the target task or used as frozen backbone encoders to provide transferable features for lightweight task-specific heads. With these strong priors, competitive models can often be obtained rapidly using only a small amount of data (Siméoni et al., 2025). Therefore, we argue that developing efficient data synthesis and training strategies tailored to such pre-trained models is a key prerequisite for advancing DD beyond a “toy” setting toward real-world applicability.

The pioneering work, Linear Gradient Matching (LGM) (Cazenavette et al., 2025), first forwards both real images and noise-initialized synthetic images through the frozen backbone of the pre-trained self-supervised model, and then optimizes the synthetic images so that they induce gradient updates on the backbone-attached linear classification head that are similar to those induced by real images. On the one hand, this batch-level process requires loading thousands of real images at each distillation step. On the other hand, each synthetic image undergoes multiple rounds of differentiable augmentations, so the *autograd* computation graphs for all views and their intermediate activations must be retained to enable backpropagation, which incurs significant computational overhead and GPU memory usage.

In this work, we delve into the mechanism of LGM. We reformulate the linear gradient into a form of local relative distribution, which we call **flow**. The flow is directed from the **target class**’s distribution center toward that of the **non-target class**. Subsequently, we reveal some key limitations (e.g., sub optimality and inefficiency) of this local matching paradigm and propose **Statistical Flow Matching (SFM)**. SFM can efficiently and effectively guides the synthesis of distilled images within a supervised learning framework, merely by statistically summarizing the distribution center of the original dataset on the distillation model once. Moreover, we recognize that models trained on highly compressed synthetic datasets often struggle to capture the decision boundaries or discriminative information acquired by models trained on the original dataset. Accordingly, we propose **Classifier Inheritance (CI)**. The specific classifier is trained on the original dataset using the distilled model. For evaluation, we only train an extremely lightweight projector consisting of a single linear layer, and then perform inference using the inherited classifier. We observe that the classifier delivers substantial performance gains, outperforming soft label guidance in both effectiveness and stability. We therefore refer to it as the **“Golden Classifier”**.

As shown in Fig. 1, by retaining only one image per class on ImageNet-100, we achieve 80%~95% validation accuracy across multiple self-supervised models by training only a linear classifier or projector. Compared to LGM, our method

reduces GPU memory usage by 10× (16 GB vs. 165 GB) and shortens the runtime by 4× (18 min vs. 80 min).

Overall, our contributions are summarized as follows:

- We identify linear gradient as local relative distribution, thereby establishing for the first time the concept of flow for dataset distillation.
- We propose statistical flow matching, a novel framework for global supervised learning that ensures stability and efficiency in the process of image synthesis.
- To the best of our knowledge, we are the first to reuse the classifier trained on the original dataset in the context of DD, achieving significant gains at minimal cost.
- Extensive experiments demonstrate that our method consistently outperforms state-of-the-art approaches in both performance and efficiency.

## 2. Related Work

**Dataset Distillation.** As the scale of datasets in machine learning continues to grow, efficient storage and learning paradigms have attracted the attention of researchers. As a result, they have shifted from the initial coresnet approach (Chen et al., 2012; Wei et al., 2015), which directly selects representative samples from the raw dataset, to dataset distillation, which generates abstract or non-original images containing insightful information from the original dataset. This has led to a range of mode, including the introduction of consistency loss that matches distribution (Li et al., 2025), gradient (Zhao et al., 2020), trajectory (Zhong et al., 2025), statistics (Shao et al., 2024), and other parameter optimization (Bao et al., 2025), generation-based approaches (Cazenavette et al., 2023; Chan-Santiago et al., 2025). However, under low-IPC settings, these methods do not perform particularly well when training models from scratch, and they also tend to have relatively high resource demands.

**Self-Supervised Learning.** Due to the expensive and time-consuming nature of collecting labeled data on a large scale in reality, self-supervised learning has become a representative method for pre-training networks, allowing models to learn transferable representations from abundant unlabeled data for subsequent downstream tasks. Widely adopted self-supervised vision models mainly include CLIP (Radford et al., 2021), DINO (Oquab et al., 2023), EVA (Fang et al., 2024), and MoCo (Chen et al., 2021).

In this work, we consider an extreme setting where we distill only **one image per class** from pre-trained self-supervised vision models, and for downstream tasks we train only a **linear classifier or a projector**. Our satisfactory results have indeed unlocked the potential of this paradigm.

### 3. Method

In this section, we deeply explore the mechanism of dataset distillation through linear gradient matching in pre-trained self-supervised vision models. We reveal its essence and the limitations it brings. Based on this, we propose SFM and CI, thereby improving distillation efficiency and performance.

#### 3.1. Rethinking Linear Gradient Matching

Formally, we consider a frozen self-supervised feature extractor  $\phi$  that maps images into a latent representation space. Given an original large-scale dataset  $\mathcal{O} = \{(\mathbf{x}_i^o, \mathbf{y}_i^o)\}_{i=1}^{|\mathcal{O}|}$ , our objective is to construct a compact synthetic dataset  $\mathcal{S} = \{(\mathbf{x}_i^s, \mathbf{y}_i^s)\}_{i=1}^{|\mathcal{S}|}$ , which enables training a linear classifier with performance on par with that trained on the full real dataset. where  $|\mathcal{S}| \ll |\mathcal{O}|$  and  $\mathbf{x}_i^o, \mathbf{x}_i^s \sim P(\mathbf{x}^o), P(\mathbf{x}^s)$  are the original and synthetic images with the corresponding one-hot labels  $\mathbf{y}_i^o, \mathbf{y}_i^s \in \mathcal{Y}$ .

To achieve this, LGM samples a **random** linear classifier matrix  $\mathbf{W} \sim \mathcal{N}(0, 0.01^2) \in \mathbb{R}^{C \times F}$  at each distillation step to enforce that training on the synthetic data mimics the gradient updates from training on real data under diverse initialization, where  $C$  is the number of classes and  $F$  is the output dimension of feature extractor  $\phi$ . After the original and synthetic images pass forward through  $\phi$  and  $\mathbf{W}$ , the gradient of the cross-entropy loss  $\ell$  with respect to  $\mathbf{W}$  is:

$$\frac{\partial \ell}{\partial \mathbf{W}} = \frac{1}{B} \sum_{i=1}^B (\mathbf{p}_i - \mathbf{y}_i) \phi(\mathbf{x}_i)^\top, \quad (1)$$

where  $B = aC$  is the batch size under the setting of IPC 1,  $a$  is the number of augmentation per batch for each class.  $\mathbf{p}_i = [p_{i1}, p_{i2}, \dots, p_{ic}, \dots, p_{iC}]$  is the probability distribution of the  $i$ -th sample:

$$p_{ic} = \text{softmax}(z_{ic}) = \frac{\exp(z_{ic})}{\sum_{j=1}^C \exp(z_{ij})}, \quad (2)$$

where  $\mathbf{z}_i = [z_{i1}, z_{i2}, \dots, z_{ic}, \dots, z_{iC}] = \mathbf{W}\phi(\mathbf{x}_i)$  is the logits of the  $i$ -th sample.

Then, the LGM loss can be defined as:

$$\mathcal{L}_{lgm} = \mathcal{M}(\frac{\partial \ell^o}{\partial \mathbf{W}}, \frac{\partial \ell^s}{\partial \mathbf{W}}), \quad (3)$$

where  $\mathcal{M}$  is the distance metrics, typically the cosine distance. The loss is subsequently backpropagated through the computational graph, which includes the inner gradient step, feature extractor, and the linear classifier, to obtain  $\frac{\partial \mathcal{L}_{lgm}}{\partial \mathbf{x}^s}$  and update the synthetic images.

For Eq. 1, given the determinism of the labels  $\mathbf{y}$  and the feature extractor  $\phi$ , the update of the synthetic data depends entirely on  $\mathbf{p}$ , which is in turn governed exclusively by the dynamic classifier's linear matrix  $\mathbf{W}$ .

**Theorem 3.1** (Exchangeability). *In a multiclass classification using the softmax function. Let the number of classes be  $C$ , and the weight vectors  $\mathbf{W}_c$  for each class  $c$  are independently initialized from a Gaussian distribution with mean zero  $\mathbf{W}_c \sim \mathcal{N}(0, \sigma_c^2)$ . For sample  $i$ , the predicted class probabilities  $p_{ic}$  for each class  $c$  are exchangeable and uniformly distributed across the classes:*

$$\mathbb{E}[p_{i1}] = \dots = \mathbb{E}[p_{ic}] = \dots = \mathbb{E}[p_{iC}] = 1/C.$$

**Theorem 3.2** (LogNormal Distribution). *Let  $Y \sim \mathcal{N}(\mu, \sigma^2)$  be a normally distributed random variable, and define  $X = e^Y$ . Then  $X$  follows a lognormal distribution, denoted  $X \sim \mathcal{LN}(\mu, \sigma^2)$ , with:*

$$\begin{aligned} \mathbb{E}[X] &= \exp(\mu + \sigma^2/2), \\ \text{Var}[X] &= \exp(2\mu + \sigma^2) [\exp(\sigma^2) - 1]. \end{aligned}$$

According to **Theorem 3.1**, the expectation of Eq. 1 is:

$$\begin{aligned} \mathbb{E}[\frac{\partial \ell}{\partial \mathbf{W}}] &= \frac{1}{B} \sum_{i=1}^B (\mathbf{p}_i - \mathbf{y}_i) \phi(\mathbf{x}_i)^\top \\ &= \frac{1}{B} \sum_{i=1}^B (\frac{1}{C} \mathbf{1} - \mathbf{y}_i) \phi(\mathbf{x}_i)^\top. \end{aligned} \quad (4)$$

We are aware that the  $c$ -th row of linear classifier matrix  $\mathbf{W}_c \sim \mathcal{N}(0, 0.01^2)$ ,  $z_{ic} = \mathbf{W}_c \phi(\mathbf{x}_i) \sim \mathcal{N}(0, \sigma^2)$  ( $\sigma = 0.01^2 \|\phi(\mathbf{x}_i)\|^2$ ). A LayerNorm operation is typically applied at the end of self-supervised models, which ensures that  $\|\phi(\mathbf{x}_i)\| = O(1)$  and  $\sigma$  has a bounded and small value.

According to **Theorem 3.2**, the expectation and variance of  $\exp(z_{ic})$  can be expresses as:

$$\begin{aligned} \mathbb{E}[\exp(z_{ic})] &= \exp(\sigma^2/2), \\ \text{Var}[\exp(z_{ic})] &= \exp(\sigma^2) \cdot [\exp(\sigma^2) - 1], \end{aligned} \quad (5)$$

When  $C$  is relatively large (e.g., 100), according to the law of large numbers  $\mathbb{E}[\exp(z_{ic})] \approx \sum_{j=1}^C \exp(z_{ij})/C$ , the variance of  $p_{ic}$  in Eq. 2 can be expressed as:

$$\begin{aligned} \text{Var}[p_{ic}] &= \text{Var}[\frac{\exp(z_{ic})}{C \cdot \exp(\sigma^2/2)}] = \frac{\text{Var}[\exp(z_{ic})]}{C^2 \exp(\sigma^2)} \\ &= \frac{\exp(\sigma^2) \cdot [\exp(\sigma^2) - 1]}{C^2 \cdot \exp(\sigma^2)} = \frac{\exp(\sigma^2) - 1}{C^2}, \end{aligned} \quad (6)$$

Since  $\sigma$  is very small, we can see that when  $C$  is relatively large,  $\text{Var}[p_{ic}] \rightarrow 0$ . From **Theorem 3.1**,  $p_{ic} \rightarrow 1/C$ , and the fluctuation is determined solely by  $\mathbf{W}$ .

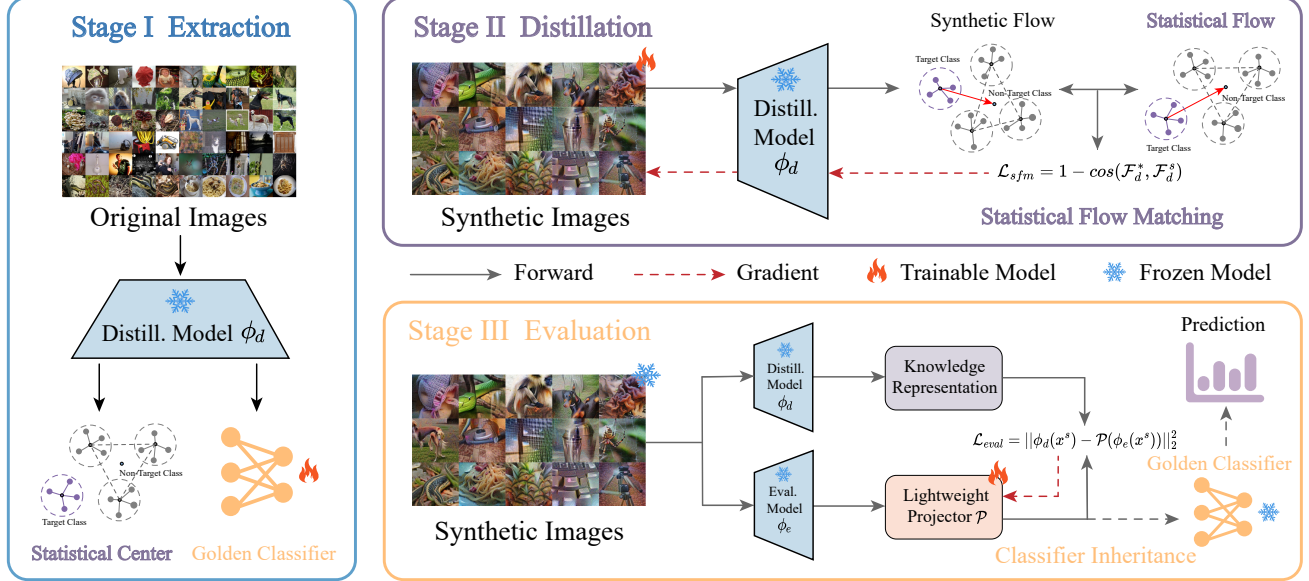


Figure 2. The framework of our method. Stage I: Given a pre-trained self-supervised vision model, we extract the global statistical center summarized from the original dataset and retain the classifier trained on that dataset, which together serve as the supervision signal for distillation and the inference head during evaluation. Stage II: We optimize the synthetic images by matching their flow through the distillation model to the statistical flow. Stage III: We only train a lightweight linear projector following the evaluation model to align the distillation model’s knowledge representation on synthetic images. Subsequently, the inherited golden classifier is used for inference and prediction.

To investigate the impact of  $\mathbf{W}$ , we establish three baselines: (1) the raw LGM with **random**  $\mathbf{W}$  sampled at every distillation step, (2) **fixed**  $\mathbf{W}$  over the whole distillation process, and (3) an **analytical** form in Eq. 4 that is independent of  $\mathbf{W}$ . As shown in Tab. 1, all modes under various models achieve similar performance, which indicates that  $\mathbf{W}$  has no significant impact on performance. This primarily stems from the fact that  $p_{ic} \rightarrow 1/C$  is weakly correlated with  $\mathbf{W}$ . Although randomly sampling  $\mathbf{W}$  intends to enhance generalization by aligning gradients under different initial conditions, both our theoretical analysis and experimental results indicate that this constitutes a redundant constraint.

Therefore, the gradient of the loss with respect to  $\mathbf{W}$  degenerates entirely into the analytical form shown in Eq. 4:

$$\begin{aligned}
 \frac{\partial \ell}{\partial \mathbf{W}_c} &= \frac{1}{B} \sum_{i=1}^B \frac{1}{C} \phi(\mathbf{x}_i | \mathbf{y}_{ic}=0)^\top - \frac{C-1}{C} \phi(\mathbf{x}_i | \mathbf{y}_{ic}=1)^\top \\
 &= \frac{1}{aC} \cdot \frac{a(C-1)}{C} \left[ \frac{\sum_{i=1}^{a(C-1)} \phi(\mathbf{x}_i | \mathbf{y}_{ic}=0)^\top}{a(C-1)} - \frac{\sum_{i=1}^a \phi(\mathbf{x}_i | \mathbf{y}_{ic}=1)^\top}{a} \right] \\
 &= \frac{C-1}{C^2} [\bar{\phi}(\mathbf{x} | \mathbf{y}_c=0)^\top - \bar{\phi}(\mathbf{x} | \mathbf{y}_c=1)^\top],
 \end{aligned} \tag{7}$$

This effectively models a pattern of relative distribution. We refer to it as **flow** and the corresponding matching strategy is called flow matching. The flow originates from the distribution center of **target class**  $\bar{\phi}(\mathbf{x} | \mathbf{y}_c=1)$  and terminates at the distribution center of **non-target class**  $\bar{\phi}(\mathbf{x} | \mathbf{y}_c=0)$ .

Table 1. A comparison of average cross-architecture performance under different  $\mathbf{W}$  settings. The number of augmentation per batch is set to 1. It proves to be insensitive to changes in  $\mathbf{W}$ .

Mode	CLIP	DINO-v2	EVA-02	MoCo-v3
Random	64.9 $\pm$ 0.2	78.3 $\pm$ 0.2	72.2 $\pm$ 0.1	72.5 $\pm$ 0.1
Fixed	64.4 $\pm$ 0.4	78.4 $\pm$ 0.2	72.6 $\pm$ 0.3	72.4 $\pm$ 0.2
Analytic	64.3 $\pm$ 0.4	78.4 $\pm$ 0.2	73.0 $\pm$ 0.1	71.9 $\pm$ 0.2

### 3.2. Statistical Flow Matching

Flow matching is invariably performed at the batch level, which results in local suboptimality. Specifically, the target and non-target class center (1) **inadequately** represent the full data distribution within a batch, leading optimization astray from the global optimum, and (2) vary dynamically across distillation steps or batches, causing optimization **instability** that induces artifacts in the synthetic images and thereby degrades performance. These also explain why LGM implicitly adopts large batch size on original data and multiple augmentations on synthetic data, which proves to be generally effective in capturing global distribution.

Additionally, (3) employing large batch size and extensive augmentations imposes substantial demands on memory and computational resources. This stems from the necessity to load large volumes of original images and maintain intricate computational graphs for gradient computation across numerous augmented synthetic images, rendering the process highly **inefficient**. Consequently, we propose a simple

but comprehensive method to simultaneously address the aforementioned three limitations.

We advocate precomputing class-wise statistical centers  $\phi^*(x)$  from the original dataset, thereby constructing a constant statistical flow  $\mathcal{F}^* = [\mathcal{F}_1^*, \dots, \mathcal{F}_c^*, \dots, \mathcal{F}_C^*]$ , where:

$$\mathcal{F}_c^* = \phi^*(\mathbf{x}^o | \mathbf{y}_c^o = 0)^\top - \phi^*(\mathbf{x}^o | \mathbf{y}_c^o = 1)^\top, \quad (8)$$

The statistical flow enables synthetic data to learn a global objective in a adequate, stable and efficient manner. Operating within a **supervised learning** paradigm, our method eliminates the need to load massive original data and perform repeated augmentations on synthetic data, significantly boosting the stability and efficiency of optimization.

Our meta loss is designed as the cosine distance between the synthetic flow  $\mathcal{F}_d^s$  and the statistical flow  $\mathcal{F}_d^*$ :

$$\mathcal{L}_{sfm} = 1 - \cos(\mathcal{F}_d^*, \mathcal{F}_d^s), \quad (9)$$

where the subscript  $d$  denotes the distillation model.

### 3.3. Classifier Inheritance

The goal of a neural network in the classification task is to learn a decision boundary that separates different classes in the feature space. In the evaluation of our downstream tasks, as the self-supervised model is frozen, the classifier uniquely learns task-specific information and determines the decision boundary. However, given that our synthetic dataset is highly compressed, such limited data is difficult to learn the decision boundary or discriminant information originally acquired by the classifier on the original dataset.

Motivated by hypothesis transfer learning (Redko et al., 2020; Chen et al., 2022), which closely matches our scene by leveraging a source-domain classifier for target-domain training with limited labeled data and no access to source data, we avoid training the target model from scratch. Instead, we inherit the pre-trained classifier  $f$  called **golden classifier** from the distillation model trained on the original dataset, and focus on learning a projector  $\mathcal{P}$ :

$$\mathcal{L}_{eval} = \|\phi_d(\mathbf{x}^s) - \mathcal{P}(\phi_e(\mathbf{x}^s))\|_2^2, \quad (10)$$

In our experiments,  $\mathcal{P}$  is extremely lightweight, consisting only of single linear layer. On the one hand, it aligns the input dimensionality of the golden classifier, and on the other hand, it learns architecture-specific knowledge from the distillation model. Such specific knowledge is crucial for cross-architecture generalization, as the images synthesized according to Eq. 9 are inherently biased toward the distillation model  $\phi_d$ , and this cannot be eliminated during evaluation. Therefore, we embrace this bias and directly learn the representations of the distillation model.

Notably, label information is no longer required for computing the loss, and the feature alignment loss in Eq. 10

becomes the only source of optimization gradients. We don't need complex fine-tuning of the hyperparameters for different loss weights like soft labels. Once the projector has been trained, we directly reuse the pre-trained golden classifier for inference on the validation images  $\mathbf{x}^v$ :

$$\mathcal{I} = f(\mathcal{P}(\phi_e(\mathbf{x}^v))), \quad (11)$$

Our CI is simple and storage-efficient, requiring only an additional classifier and one image per class to be stored. This design is well suited to bandwidth-limited weakly connected settings and resource-constrained edge environments.

## 4. Experiments

**Datasets and Backbones.** To evaluate the effectiveness of our method, we conduct all experiments on various datasets with  $224 \times 224$  resolution, including universal ImageNet-1k (Deng et al., 2009) and ImageNet-100 (Chan-Santiago et al., 2025), fine-grained Stanford Dogs (Dataset, 2011) and CUB-200-2011 (Welinder et al., 2010), and other ImageWoof (Howard, 2019) and ArtBench (Liao et al., 2022) datasets used for ablation and expansion research. We mainly use the “ViT-B” version of four pre-trained self-supervised models or feature extractors as backbones: CLIP (Radford et al., 2021), DINO-v2 (Oquab et al., 2023), EVA-02 (Fang et al., 2024), and MoCo-v3 (Chen et al., 2021).

**Baselines and Evaluation.** We compare our method with the state-of-the-art method LGM (Cazenavette et al., 2025) and three real-image baselines, including Random (simply select a random image for each class), Centroids (take the real image closest to the mean embedding for each class), and Neighbors (choose the real image with the minimum embedding distance to the synthetic image). We use only the final layer of the backbone network to provide transferable features for the task-specific classification head. The lightweight projector consists of only a single linear layer, comparable to the weight parameters of the classifier. The reported results represent the averages of 3 trials for ImageNet-1k and 5 trials for other datasets.

**Implementation details.** Following LGM, we train the pyramid representations (Fort & Whitaker, 2025) with Adam optimizer (Adam et al., 2014) at a learning rate of 0.002. We distill the synthetic images for 5000 iterations, adding a new level to the pyramid every 200 iterations. A single differentiable augmentation (Zhao & Bilen, 2021) is applies to our synthetic images, while LGM uses 3 augmentations for ImageNet-1k and 10 for other datasets. During evaluation, we evaluate synthetic images for 1000 iterations (with convergence typically occurring in just a few minutes, within 100~200 iterations). The vanilla classifier uses a learning rate of 0.001, while our projector uses 0.01. All experiments are conducted on a single H100 GPU, except for the ImageNet-1K dataset, which is run on two GPUs.

**Table 2. The distillation performance on specific models.** We compare our method (SFM and CI) with LGM and several real-image baselines on ImageNet-100, ImageNet-1k, Stanford Dogs and CUB-200. Our SFM achieves results that are equal to or better than those of LGM with multiple augmentations using only a single augmentation, and consistently outperforms all other real baselines. Combining our CI with SFM yields substantial performance gains, achieving comparable performance to training on the full dataset. The best results are **bolded**, and the second best results are emphasized in underlined case. The same applies below.

Train Set (1 Img/Clss)	ImageNet-100					ImageNet-1k				
	CLIP	DINO-v2	EVA-02	MoCo-v3	Average	CLIP	DINO-v2	EVA-02	MoCo-v3	Average
Random	<b>56.6</b> $\pm$ 1.6	74.8 $\pm$ 2.8	64.5 $\pm$ 2.7	61.4 $\pm$ 2.6	64.3 $\pm$ 2.4	31.7 $\pm$ 0.5	50.3 $\pm$ 0.5	37.7 $\pm$ 0.4	38.8 $\pm$ 0.6	39.6 $\pm$ 0.5
Centroids	77.1 $\pm$ 0.1	86.9 $\pm$ 0.3	80.9 $\pm$ 0.2	77.7 $\pm$ 0.1	80.6 $\pm$ 0.2	53.9 $\pm$ 0.0	69.5 $\pm$ 0.1	58.1 $\pm$ 0.1	57.4 $\pm$ 0.0	59.7 $\pm$ 0.1
Neighbors (LGM)	67.8 $\pm$ 0.3	86.0 $\pm$ 0.2	78.8 $\pm$ 0.2	77.1 $\pm$ 0.1	77.4 $\pm$ 0.2	38.8 $\pm$ 0.1	67.7 $\pm$ 0.1	49.9 $\pm$ 0.1	56.4 $\pm$ 0.0	53.2 $\pm$ 0.1
Neighbors (SFM)	72.2 $\pm$ 0.2	88.0 $\pm$ 0.1	80.4 $\pm$ 0.0	77.8 $\pm$ 0.1	79.6 $\pm$ 0.1	48.1 $\pm$ 0.1	69.6 $\pm$ 0.0	57.3 $\pm$ 0.0	57.0 $\pm$ 0.0	58.0 $\pm$ 0.0
LGM	84.9 $\pm$ 0.1	<b>91.5</b> $\pm$ 0.1	<u>89.0</u> $\pm$ 0.0	83.4 $\pm$ 0.1	87.2 $\pm$ 0.1	63.0 $\pm$ 0.0	75.0 $\pm$ 0.1	70.3 $\pm$ 0.1	63.2 $\pm$ 0.0	67.9 $\pm$ 0.0
Ours (SFM)	86.7 $\pm$ 0.1	90.6 $\pm$ 0.0	88.9 $\pm$ 0.2	84.7 $\pm$ 0.0	87.7 $\pm$ 0.1	<u>67.1</u> $\pm$ 0.0	75.1 $\pm$ 0.1	71.6 $\pm$ 0.1	63.4 $\pm$ 0.0	69.3 $\pm$ 0.1
Ours (SFM+CI)	<b>92.2</b> $\pm$ 0.1	<b>95.1</b> $\pm$ 0.1	<b>93.1</b> $\pm$ 0.1	<b>87.5</b> $\pm$ 0.0	<b>92.0</b> $\pm$ 0.1	<b>78.0</b> $\pm$ 0.1	<b>82.0</b> $\pm$ 0.0	<b>79.3</b> $\pm$ 0.1	<b>74.0</b> $\pm$ 0.0	<b>78.3</b> $\pm$ 0.1
Full Dataset	92.5 $\pm$ 0.0	95.2 $\pm$ 0.1	94.1 $\pm$ 0.1	89.4 $\pm$ 0.3	92.8 $\pm$ 0.1	78.7 $\pm$ 0.0	83.0 $\pm$ 0.0	81.7 $\pm$ 0.1	76.5 $\pm$ 0.0	80.0 $\pm$ 0.0
Train Set (1 Img/Clss)	Stanford Dogs					CUB-200				
	CLIP	DINO-v2	EVA-02	MoCo-v3	Average	CLIP	DINO-v2	EVA-02	MoCo-v3	Average
Random	23.3 $\pm$ 1.5	51.9 $\pm$ 1.8	38.3 $\pm$ 1.8	36.6 $\pm$ 1.4	37.5 $\pm$ 1.6	37.5 $\pm$ 1.6	64.4 $\pm$ 1.5	44.3 $\pm$ 1.5	19.1 $\pm$ 0.5	41.3 $\pm$ 1.3
Centroids	43.3 $\pm$ 0.1	73.0 $\pm$ 0.2	60.9 $\pm$ 0.2	55.2 $\pm$ 0.2	58.1 $\pm$ 0.2	54.3 $\pm$ 0.2	78.5 $\pm$ 0.2	59.9 $\pm$ 0.3	30.2 $\pm$ 0.1	55.7 $\pm$ 0.2
Neighbors (LGM)	33.4 $\pm$ 0.1	71.3 $\pm$ 0.2	58.5 $\pm$ 0.2	56.3 $\pm$ 0.1	54.9 $\pm$ 0.2	39.4 $\pm$ 0.1	76.9 $\pm$ 0.0	52.6 $\pm$ 0.3	28.1 $\pm$ 0.0	49.2 $\pm$ 0.1
Neighbors (SFM)	35.7 $\pm$ 0.1	72.3 $\pm$ 0.2	60.3 $\pm$ 0.2	55.5 $\pm$ 0.3	56.0 $\pm$ 0.2	47.3 $\pm$ 0.3	78.7 $\pm$ 0.1	56.0 $\pm$ 0.2	28.7 $\pm$ 0.1	52.7 $\pm$ 0.2
LGM	52.1 $\pm$ 0.2	<u>83.0</u> $\pm$ 0.1	74.8 $\pm$ 0.1	69.6 $\pm$ 0.2	69.9 $\pm$ 0.2	62.2 $\pm$ 0.2	86.0 $\pm$ 0.1	74.1 $\pm$ 0.2	42.5 $\pm$ 0.2	66.2 $\pm$ 0.2
Ours (SFM)	55.0 $\pm$ 0.3	81.8 $\pm$ 0.2	72.9 $\pm$ 0.2	67.2 $\pm$ 0.3	69.2 $\pm$ 0.3	67.6 $\pm$ 0.2	85.7 $\pm$ 0.1	72.5 $\pm$ 0.2	41.4 $\pm$ 0.1	66.8 $\pm$ 0.2
Ours (SFM+CI)	<b>62.4</b> $\pm$ 0.4	<b>85.5</b> $\pm$ 0.3	<b>78.7</b> $\pm$ 0.1	<b>70.0</b> $\pm$ 0.1	<b>74.2</b> $\pm$ 0.2	<b>68.4</b> $\pm$ 0.5	<b>88.1</b> $\pm$ 0.3	<b>79.7</b> $\pm$ 0.1	<b>43.3</b> $\pm$ 0.1	<b>69.9</b> $\pm$ 0.3
Full Dataset	76.9 $\pm$ 0.1	88.6 $\pm$ 0.1	82.6 $\pm$ 0.1	72.3 $\pm$ 0.5	80.1 $\pm$ 0.2	77.5 $\pm$ 0.7	90.2 $\pm$ 0.2	84.0 $\pm$ 0.3	43.7 $\pm$ 0.8	73.8 $\pm$ 0.5

**Table 3.** The effects of Target Class (TCDD) and Non-target Class (NCDD) Dataset Distillation. The results represent the average cross-architecture generalization performance distilled from CLIP.

TCDD	NCDD	IN-Woof	IN-100	IN-1k
$\times$	✓	16.0 $\pm$ 1.0	0.77 $\pm$ 0.0	0.10 $\pm$ 0.1
✓	$\times$	<b>84.9</b> $\pm$ 0.5	79.4 $\pm$ 0.1	57.9 $\pm$ 0.0
✓	✓	81.8 $\pm$ 0.9	<b>81.5</b> $\pm$ 0.2	<b>60.6</b> $\pm$ 0.0

#### 4.1. Distillation Performance on Specific Models

As shown in Tab. 2, we distill synthetic images using diverse backbones and evaluate them under consistent architectures. With only a single augmentation, SFM achieves performance comparable to or better than LGM, and substantially outperforms other real-image baselines. Notably, our synthetic Neighbors are generally superior to those of LGM, indirectly indicating that our images reside in a more representative feature space of the entire dataset. We also observe that DINO serves as a particularly effective backbone, achieving the best performance across all datasets, likely due to its unique self-distillation paradigm.

Furthermore, CI yields remarkable additional gains, even approaching the performance of training on the full dataset. This demonstrates that the golden classifiers, which possess distinct discriminative capabilities, are crucial for training with our extremely compressed synthetic data.

#### 4.2. Generalization Performance Across Models

Next, we evaluate the cross-model generalization performance on ImageNet-100. As depicted in Tab. 4, the generalization performance of our SFM generally surpasses that of LGM. For instance, under the EVA-02 and CLIP model pair, SFM achieves a 5.5% improvement (81% vs. 75.5%). The introduction of CI also leads to a significant improvement.

We observe that (1) the generalization performance of DINO-v2 remains at the highest level, and (2) even when evaluating images distilled using the same model, the performance gap remains significant across different models. For example, when MoCo-v3 is used as the distillation model, DINO-v2 can reach 86.6%, while CLIP is only 66.3% which is far inferior to other real-image baselines. Both cases indicate that the type and quality of self-supervised models can affect the generalization ability of the synthetic dataset.

#### 4.3. Ablation Analysis

**Target Class and Non-target Class.** We distill synthetic images using the two parts in Eq. 7 separately, termed as Target Class Dataset Distillation (TCDD) and Non-target Class Dataset Distillation (NCDD). As shown in Tab. 3, NCDD individually collapses across all dataset scales. In contrast, TCDD alone outperforms our SFM (TCDD+NCDD) on the small-scale ImageWoof with only 10 classes, indicating that preserving basic representative features (distribution

**Table 4. The generalization performance across models.** We synthesize images using a given model and then evaluate them across all models on ImageNet-100. Our distilled datasets also generalize well across different model pairs. While there remains a performance gap between the CI-enhanced method and training on the full dataset, it still delivers significant improvement compared to the raw SFM.

Distill. Model		CLIP					DINO-v2				
Eval. Model	CLIP	DINO-v2	EVA-02	MoCo-v3	Average	CLIP	DINO-v2	EVA-02	MoCo-v3	Average	
Centroids	77.1 $\pm$ 0.1	85.1 $\pm$ 0.2	82.6 $\pm$ 0.2	74.7 $\pm$ 0.1	79.9 $\pm$ 0.2	72.4 $\pm$ 0.0	86.9 $\pm$ 0.3	80.1 $\pm$ 0.4	75.8 $\pm$ 0.1	78.8 $\pm$ 0.2	
Neighbors (LGM)	67.8 $\pm$ 0.3	81.1 $\pm$ 0.1	75.0 $\pm$ 0.2	70.4 $\pm$ 0.0	73.5 $\pm$ 0.1	71.2 $\pm$ 0.1	86.0 $\pm$ 0.2	78.0 $\pm$ 0.4	74.7 $\pm$ 0.0	77.6 $\pm$ 0.2	
Neighbors (SFM)	72.2 $\pm$ 0.2	83.6 $\pm$ 0.2	75.8 $\pm$ 0.0	72.3 $\pm$ 0.1	76.0 $\pm$ 0.1	72.7 $\pm$ 0.0	88.0 $\pm$ 0.1	80.0 $\pm$ 0.2	75.4 $\pm$ 0.0	79.0 $\pm$ 0.1	
LGM	84.9 $\pm$ 0.1	80.8 $\pm$ 0.4	83.8 $\pm$ 0.2	61.6 $\pm$ 0.2	77.8 $\pm$ 0.2	77.0 $\pm$ 0.1	91.5 $\pm$ 0.1	86.8 $\pm$ 0.1	78.8 $\pm$ 0.1	83.5 $\pm$ 0.1	
Ours (SFM)	86.7 $\pm$ 0.1	84.9 $\pm$ 0.3	85.5 $\pm$ 0.2	68.7 $\pm$ 0.0	81.5 $\pm$ 0.2	78.6 $\pm$ 0.0	90.6 $\pm$ 0.0	86.2 $\pm$ 0.1	80.5 $\pm$ 0.0	84.0 $\pm$ 0.0	
Ours (SFM+CI)	92.2 $\pm$ 0.1	86.0 $\pm$ 0.1	87.7 $\pm$ 0.0	73.4 $\pm$ 0.1	84.8 $\pm$ 0.1	82.1 $\pm$ 0.0	95.1 $\pm$ 0.1	88.8 $\pm$ 0.1	80.6 $\pm$ 0.1	86.7 $\pm$ 0.1	
Distill. Model		EVA-02					MoCo-v3				
Eval. Model	CLIP	DINO-v2	EVA-02	MoCo-v3	Average	CLIP	DINO-v2	EVA-02	MoCo-v3	Average	
Centroids	70.7 $\pm$ 0.1	85.2 $\pm$ 0.1	80.9 $\pm$ 0.2	72.6 $\pm$ 0.1	77.4 $\pm$ 0.1	75.5 $\pm$ 0.2	85.8 $\pm$ 0.1	81.7 $\pm$ 0.1	77.7 $\pm$ 0.1	80.2 $\pm$ 0.1	
Neighbors (LGM)	69.5 $\pm$ 0.1	85.4 $\pm$ 0.3	78.8 $\pm$ 0.2	72.3 $\pm$ 0.1	76.5 $\pm$ 0.2	72.6 $\pm$ 0.3	86.2 $\pm$ 0.2	81.1 $\pm$ 0.5	77.1 $\pm$ 0.1	79.7 $\pm$ 0.3	
Neighbors (SFM)	69.4 $\pm$ 0.3	85.2 $\pm$ 0.1	80.4 $\pm$ 0.0	74.7 $\pm$ 0.1	77.4 $\pm$ 0.1	75.8 $\pm$ 0.0	85.7 $\pm$ 0.1	81.2 $\pm$ 0.1	77.8 $\pm$ 0.1	80.1 $\pm$ 0.1	
LGM	75.5 $\pm$ 0.2	86.4 $\pm$ 0.1	89.0 $\pm$ 0.0	67.7 $\pm$ 0.1	79.7 $\pm$ 0.1	65.6 $\pm$ 0.1	86.6 $\pm$ 0.1	82.3 $\pm$ 0.2	83.4 $\pm$ 0.1	79.5 $\pm$ 0.1	
Ours (SFM)	81.0 $\pm$ 0.2	88.0 $\pm$ 0.2	88.9 $\pm$ 0.2	70.5 $\pm$ 0.0	82.1 $\pm$ 0.2	66.3 $\pm$ 0.1	86.7 $\pm$ 0.2	79.3 $\pm$ 0.2	84.7 $\pm$ 0.0	79.3 $\pm$ 0.1	
Ours (SFM+CI)	85.0 $\pm$ 0.0	88.7 $\pm$ 0.0	93.1 $\pm$ 0.0	77.6 $\pm$ 0.3	86.1 $\pm$ 0.1	71.7 $\pm$ 0.4	88.0 $\pm$ 0.1	84.4 $\pm$ 0.1	87.5 $\pm$ 0.0	82.9 $\pm$ 0.2	
Full Dataset	92.5 $\pm$ 0.0	95.2 $\pm$ 0.1	94.1 $\pm$ 0.1	89.4 $\pm$ 0.3	92.8 $\pm$ 0.1	92.5 $\pm$ 0.0	95.2 $\pm$ 0.1	94.1 $\pm$ 0.1	89.4 $\pm$ 0.3	92.8 $\pm$ 0.1	

**Table 5.** The impact of different training strategies on performance. “Vanilla” denotes training the classification head with random initialization solely on the synthetic images generated by SFM. The distillation model is CLIP.

Strategy	CLIP	DINO-v2	EVA-02	MoCo-v3
Vanilla	86.7 $\pm$ 0.1	84.9 $\pm$ 0.3	85.5 $\pm$ 0.2	68.7 $\pm$ 0.0
JT (w/o IP)	83.8 $\pm$ 0.3	85.6 $\pm$ 0.2	84.2 $\pm$ 0.1	52.5 $\pm$ 0.4
JT (w/ IP)	85.8 $\pm$ 0.1	73.4 $\pm$ 0.5	80.8 $\pm$ 0.1	65.5 $\pm$ 0.0
ST (w/o IP)	86.9 $\pm$ 0.1	85.6 $\pm$ 0.0	86.2 $\pm$ 0.1	72.5 $\pm$ 0.1
ST (w/ IP)	91.6 $\pm$ 0.1	86.2 $\pm$ 0.1	87.2 $\pm$ 0.0	74.1 $\pm$ 0.1
Our CI	92.2 $\pm$ 0.1	86.0 $\pm$ 0.1	87.7 $\pm$ 0.0	73.4 $\pm$ 0.1

centers) is sufficient for distilling compact datasets. However, when handling large-scale datasets, our flow matching demonstrates greater insight and delivers superior performance gains. A detailed analysis will be provided in the subsequent **Visualization** section.

**Golden Classifier.** To better understand CI’s key role, we design different training strategies for the classifier and projector, including **Joint Training (JT)** and **Sequential Training (ST)**. JT indicates that we train the classifier and its associated projector simultaneously. ST refers to first training the projector using the loss in Eq. 10 and then freeze it, followed by further training of the classifier. Additionally, we have set a switch on whether to inherit the **Initial Parameters (IP)** of the golden classifier. As presented in Tab. 5, regardless of whether IP is used or not, JT consistently underperforms and is even inferior to the Vanilla. In contrast, ST yields measurable gains, which is mainly because both the synthetic dataset and the golden classifier are trained on the distillation model. Therefore, aligning features with the

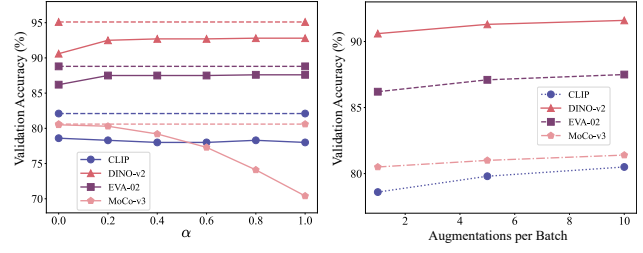


**Figure 3.** (left) A comparison between soft label training (solid line) and our CI training (dashed line). (right) The effect of applying multi-round differentiable augmentation to our synthetic data.

distillation model essentially narrows the gap between the distillation and evaluation model, which benefits classifier training on synthetic images. Notably, ST (w/ IP) achieves performance comparable to CI, indicating that the parameters of the golden classifier provide a favorable decision boundary, and further optimization based on this foundation can lead to even better performance ( $74.1\% > 73.4\%$ ).

**Soft Label.** The soft label (Qin et al., 2024; Sun et al., 2024) has been widely established as an effective evaluation method for DD. In Fig. 3 (left), we train our classifier using a weighted loss  $\alpha\ell_{kl} + (1-\alpha)\ell_{ce}$ , where soft labels are provided by the distillation model along with its corresponding classifier. We observe that soft labels are highly architecture-sensitive. While they improve performance for DINO-v2 and EVA-02, they provide no benefit for CLIP and even degrade results for MoCo-v3, as performance drops sharply with increased KL loss weight  $\alpha$ . Overall, CI consistently outperforms soft labels, confirming that our golden classifier is crucial for downstream training on synthetic data.



Figure 4. (Left) A comparison between images synthesized by LGM and our SFM. LGM produces images with noticeable artifacts, whereas ours are notably clearer. (Right) A comparison between images synthesized by TCDD and NCDD. TCDD effectively captures discriminative features of the target class, while NCDD deviates entirely from the target-class representation.

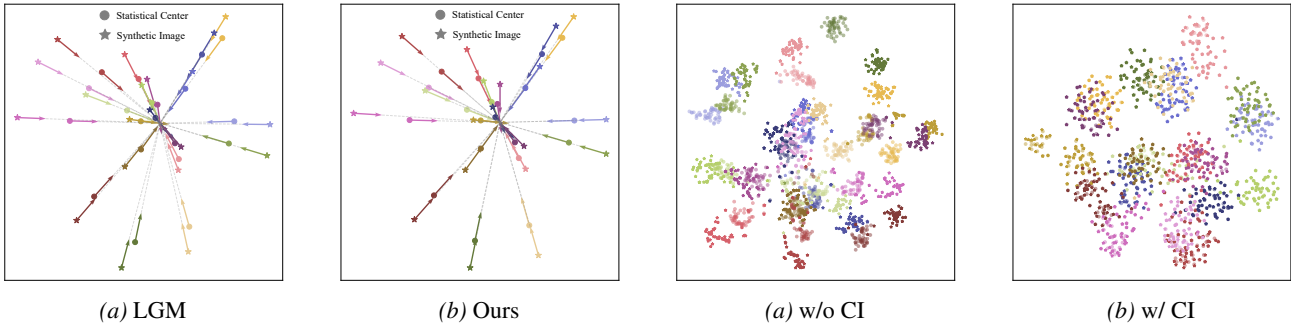


Figure 5. The flow on the ImageNet-100. We perform PCA for dimensionality reduction, visualizing 20 classes. Compared to LGM, our synthetic flow aligns more closely with the global statistical flow. Cosine similarity between the synthetic and statistical flow for all samples is 88.2 and 95.6 in the two cases, respectively.

**Differentiable Augmentation.** As shown in Fig. 3 (right), we apply more rounds of differentiable augmentation per distillation step, which boosts both distillation and generalization performance of the synthetic images. In practical applications, we can flexibly choose the augmentation rounds based on the trade-off between resources and performance.

**Visualizations.** We present multiple visualization results to demonstrate the interpretability of our method. As shown in Fig. 4 (left), our synthetic images are clearer than those of LGM and exhibit no noticeable artifacts, indicating the stability of our global-level SFM during the optimization process. In Fig. 4 (right), TCDD synthesizes images relevant to the target class, while NCDD produces unrelated non-target class that harm performance. As shown in Fig. 5, compared to the dynamic process of LGM, our synthetic flow is closer to the global statistical flow. This further confirms that our supervised paradigm effectively ensures stable global optimization. Notably, our synthetic images are generally far from the statistical centers and non-target class centers, indicating that the synthetic images have the attributes of marginal distribution and large inter-class distances, which is also why our method is more effective. Additionally, the results in Fig. 6 denote that CI indeed facilitates the generation of similar classification boundaries.

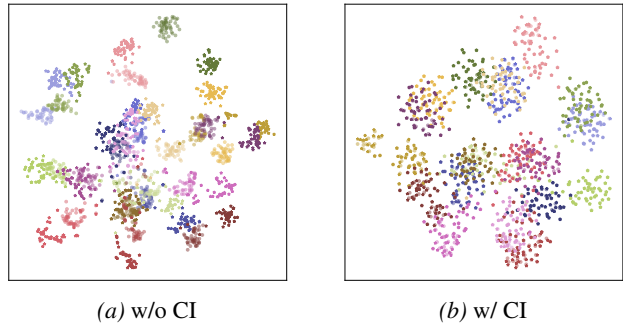


Figure 6. Visualization of test images from 20 classes of ImageNet-100 using t-SNE. The logit features extracted by the distillation and evaluation models with the classifier are depicted with circles and pentagrams, respectively. They have almost identical decision boundaries that cannot be distinguished with our CI.

## 5. Conclusion

In this work, we introduce a novel paradigm called statistical flow matching for dataset distillation, which encourages the synthetic images to efficiently learn the statistical flow of the original dataset through the pre-trained self-supervised vision model. Furthermore, for the first time, we inherit the classifier trained on the original dataset for inference and use the distilled model’s knowledge for supervising, achieving better performance than other baselines and outperforming soft labels. For example, a DINO-v2 linear classifier to reach 95.1% distillation accuracy and 86.7% generalization accuracy on ImageNet-100 within only few minutes, despite only being trained on one labeled image per class.

**Impact and Future Works.** We extract only one image per class using an efficient paradigm and save them along with an additional classifier, making it lightweight and capable of quickly training a competitive model. This has a positive impact on future edge environments with limitations in computation, storage, and communication. In future work, we plan to extend our method to object detection and semantic segmentation, where a small dataset is distilled on a self-supervised model, and their task-specific head trained on the original dataset will be retained for downstream tasks.

## References

Adam, K. D. B. J. et al. A method for stochastic optimization. *arXiv preprint arXiv:1412.6980*, 1412(6), 2014.

Bao, Y., Liu, Y., Chen, Z., Liang, Y., Li, M., and Ma, K. Dataset distillation as data compression: A rate-utility perspective. In *Proceedings of the IEEE/CVF International Conference on Computer Vision*, pp. 519–529, 2025.

Cazenavette, G., Wang, T., Torralba, A., Efros, A. A., and Zhu, J.-Y. Dataset distillation by matching training trajectories. In *Proceedings of the IEEE/CVF Conference on Computer Vision and Pattern Recognition*, pp. 4750–4759, 2022.

Cazenavette, G., Wang, T., Torralba, A., Efros, A. A., and Zhu, J.-Y. Generalizing dataset distillation via deep generative prior. In *Proceedings of the IEEE/CVF Conference on Computer Vision and Pattern Recognition*, pp. 3739–3748, 2023.

Cazenavette, G., Torralba, A., and Sitzmann, V. Dataset distillation for pre-trained self-supervised vision models. *NeurIPS*, 2025.

Chan-Santiago, J. A., Tirupattur, P., Nayak, G. K., Liu, G., and Shah, M. Mgd<sup>3</sup>: Mode-guided dataset distillation using diffusion models. *ICML*, 2025.

Chen, D., Mei, J.-P., Zhang, H., Wang, C., Feng, Y., and Chen, C. Knowledge distillation with the reused teacher classifier. In *Proceedings of the IEEE/CVF conference on computer vision and pattern recognition*, pp. 11933–11942, 2022.

Chen, X., Xie, S., and He, K. An empirical study of training self-supervised vision transformers. In *Proceedings of the IEEE/CVF international conference on computer vision*, pp. 9640–9649, 2021.

Chen, Y., Welling, M., and Smola, A. Super-samples from kernel herding. *arXiv preprint arXiv:1203.3472*, 2012.

Dataset, E. Novel datasets for fine-grained image categorization. In *First workshop on fine grained visual categorization, CVPR. Citeseer. Citeseer*, volume 5, pp. 2. Citeseer, 2011.

Deng, J., Dong, W., Socher, R., Li, L.-J., Li, K., and Fei-Fei, L. Imagenet: A large-scale hierarchical image database. In *2009 IEEE conference on computer vision and pattern recognition*, pp. 248–255. Ieee, 2009.

Du, J., Jiang, Y., Tan, V. Y., Zhou, J. T., and Li, H. Minimizing the accumulated trajectory error to improve dataset distillation. In *Proceedings of the IEEE/CVF conference on computer vision and pattern recognition*, pp. 3749–3758, 2023.

Fang, Y., Sun, Q., Wang, X., Huang, T., Wang, X., and Cao, Y. Eva-02: A visual representation for neon genesis. *Image and Vision Computing*, 149:105171, 2024.

Fort, S. and Whitaker, J. Direct ascent synthesis: Revealing hidden generative capabilities in discriminative models. *arXiv preprint arXiv:2502.07753*, 2025.

Howard, J. A smaller subset of 10 easily classified classes from imagenet, and a little more french. *URL https://github.com/fastai/imagenette*, 4, 2019.

Lei, S. and Tao, D. A comprehensive survey of dataset distillation. *IEEE Transactions on Pattern Analysis and Machine Intelligence*, 46(1):17–32, 2023.

Li, H., Zhou, Y., Gu, X., Li, B., and Wang, W. Diversity-enhanced distribution alignment for dataset distillation. In *Proceedings of the IEEE/CVF International Conference on Computer Vision*, pp. 3747–3756, 2025.

Liao, P., Li, X., Liu, X., and Keutzer, K. The artbench dataset: Benchmarking generative models with artworks. *arXiv preprint arXiv:2206.11404*, 2022.

Quab, M., Dariseti, T., Moutakanni, T., Vo, H., Szafraniec, M., Khalidov, V., Fernandez, P., Haziza, D., Massa, F., El-Nouby, A., et al. Dinov2: Learning robust visual features without supervision. *arXiv preprint arXiv:2304.07193*, 2023.

Qin, T., Deng, Z., and Alvarez-Melis, D. A label is worth a thousand images in dataset distillation. *Advances in Neural Information Processing Systems*, 37:131946–131971, 2024.

Radford, A., Kim, J. W., Hallacy, C., Ramesh, A., Goh, G., Agarwal, S., Sastry, G., Askell, A., Mishkin, P., Clark, J., et al. Learning transferable visual models from natural language supervision. In *International conference on machine learning*, pp. 8748–8763. PMLR, 2021.

Redko, I., Morvant, E., Habrard, A., Sebban, M., and Bennani, Y. A survey on domain adaptation theory: learning bounds and theoretical guarantees. *arXiv preprint arXiv:2004.11829*, 2020.

Shao, S., Yin, Z., Zhou, M., Zhang, X., and Shen, Z. Generalized large-scale data condensation via various backbone and statistical matching. In *Proceedings of the IEEE/CVF Conference on Computer Vision and Pattern Recognition*, pp. 16709–16718, 2024.

Siméoni, O., Vo, H. V., Seitzer, M., Baldassarre, F., Quab, M., Jose, C., Khalidov, V., Szafraniec, M., Yi, S., Ramamonjisoa, M., Massa, F., Haziza, D., Wehrstedt, L., Wang, J., Dariseti, T., Moutakanni, T., Sentana, L., Roberts, C., Vedaldi, A., Tolan, J., Brandt, J., Couprie, C., Mairal, J.,

Jégou, H., Labatut, P., and Bojanowski, P. DINOv3, 2025.  
URL <https://arxiv.org/abs/2508.10104>.

Su, D., Hou, J., Gao, W., Tian, Y., and Tang, B. D<sup>4</sup>m: Dataset distillation via disentangled diffusion model. In *Proceedings of the IEEE/CVF Conference on Computer Vision and Pattern Recognition*, pp. 5809–5818, 2024.

Sun, P., Shi, B., Yu, D., and Lin, T. On the diversity and realism of distilled dataset: An efficient dataset distillation paradigm. In *Proceedings of the IEEE/CVF Conference on Computer Vision and Pattern Recognition*, pp. 9390–9399, 2024.

Wang, S., Yang, Y., Liu, Z., Sun, C., Hu, X., He, C., and Zhang, L. Dataset distillation with neural characteristic function: A minmax perspective. In *Proceedings of the Computer Vision and Pattern Recognition Conference*, pp. 25570–25580, 2025.

Wang, T., Zhu, J.-Y., Torralba, A., and Efros, A. A. Dataset distillation. *arXiv preprint arXiv:1811.10959*, 2018.

Wei, K., Iyer, R., and Bilmes, J. Submodularity in data subset selection and active learning. In *International conference on machine learning*, pp. 1954–1963. PMLR, 2015.

Welinder, P., Branson, S., Mita, T., Wah, C., Schroff, F., Belongie, S., and Perona, P. Caltech-ucsd birds 200. 2010.

Yin, Z., Xing, E., and Shen, Z. Squeeze, recover and relabel: Dataset condensation at imagenet scale from a new perspective. *Advances in Neural Information Processing Systems*, 36:73582–73603, 2023.

Zhao, B. and Bilen, H. Dataset condensation with differentiable siamese augmentation. In *International Conference on Machine Learning*, pp. 12674–12685. PMLR, 2021.

Zhao, B. and Bilen, H. Dataset condensation with distribution matching. In *Proceedings of the IEEE/CVF Winter Conference on Applications of Computer Vision*, pp. 6514–6523, 2023.

Zhao, B., Mopuri, K. R., and Bilen, H. Dataset condensation with gradient matching. *arXiv preprint arXiv:2006.05929*, 2020.

Zhong, W., Tang, H., Zheng, Q., Xu, M., Hu, Y., and Guan, W. Towards stable and storage-efficient dataset distillation: Matching convexified trajectory. In *Proceedings of the Computer Vision and Pattern Recognition Conference*, pp. 25581–25589, 2025.